Fault plane solutions of crustal earthquakes in Southern Italy (1988-1995): seismotectonic implications

Alberto Frepoli and Alessandro Amato
Istituto Nazionale di Geofisica, Roma, Italy

Abstract
The Southern Apennines and the Sicilian-Calabrian regions belong to the complex geodynamic Central Mediterranean area, which is dominated by the NNW-SSE convergence of the European and African plates and is strongly affected by the presence of Neogene-Quaternary subduction/collision arcs and related back-arc basins. In order to obtain a more detailed picture of the processes active in these two regions, we calculated 173 new fault plane solutions of crustal events with $2.5 < M < 4.4$ recorded by the national seismic network of the Istituto Nazionale di Geofisica in the period 1988-1995. Normal and strike-slip solutions are largely prevalent in the Southern Apennines, with tensional (T) axes mostly oriented NE-SW, perpendicular to the belt, in agreement with active stress directions from breakouts. In the Sicilian region the seismicity is concentrated in the eastern portion of the island. Different focal mechanism categories are present in the Nebrodi and Etna sector indicating a complex strain release in these two regions. Thrust and strike-slip solutions prevail in the Aeolian Islands associated with ~ N-S compression, whereas in Western Sicily the prevailing orientation of P-axes is around WNW-ESE. Although not well constrained due to only a few data in the region, there is a hint of active compression at the outer front of the Calabrian arc, in the Ionian Sea. The observed pattern of fault plane solutions suggests that the transition between oceanic subduction beneath Calabria and continental subduction in Sicily and in Southern Apennines controls the active tectonics of Southern Italy.

Key words *Southern Italy – focal mechanisms – seismicity – stress distribution*

1. Introduction

The Southern Apennines are characterized by NW-SE compressional and extensional structures developed since Miocene times. The deformed Meso-Cenozoic sedimentary units which form the Apenninic thrust and fold belt were emplaced by the eastward migration of the «extension-compression» system drived by the subduction process of the Ionian-Adriatic plate related with the opening of the Tyrrhenian Sea (Malinverno and Ryan, 1986; Philip, 1987; Royden *et al.*, 1987) (fig. 1). This opening started in Late Tortonian (~ 7 Ma) with the SE migration of the Calabrian arc (Patacca and Scandone, 1989). The age of thrusting is progressively younger from the internal to the more external sedimentary units of the Southern Apennines. Since the Early Pliocene the Tyrrhenian margin began to be affected by the extensional processes still active today, while the compressional front was migrating to the east. The present NE-SW extension perpendicular to the Apenninic fold and thrust belt is well known from the normal faulting focal mechanisms of large earthquakes ($M > 5$) reported in the Centroid Moment Tensor (CMT) catalog of Harvard

Mailing address: Dr. Alberto Frepoli, Istituto Nazionale di Geofisica, Via di Vigna Murata 605, 00143 Roma, Italy; e-mail: frepoli@ingrm.it

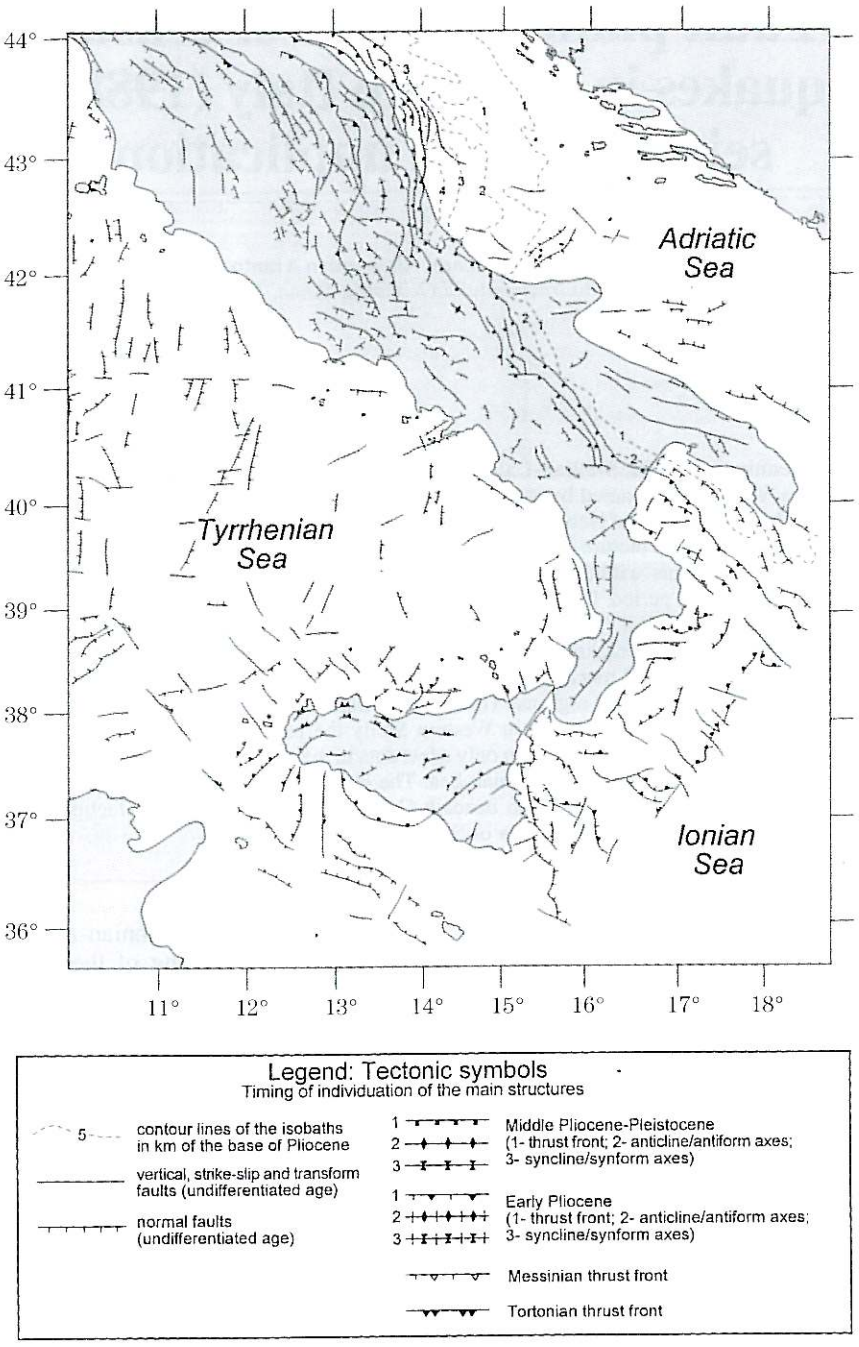

Fig. 1. Structural-kinematic map of Southern Italy (simplified from «Structural model of Italy», Bigi *et al.*, 1983).

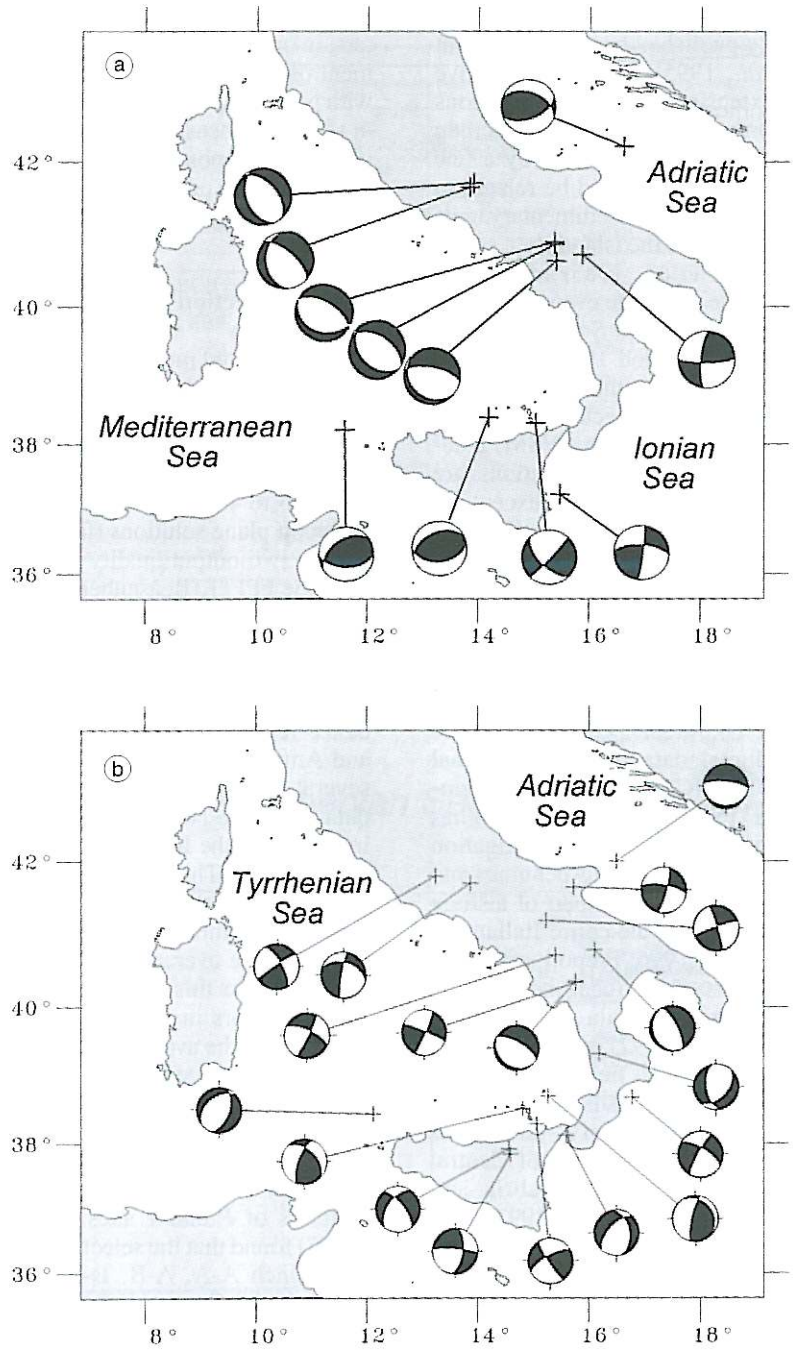

Fig. 2a,b. a) CMT solutions (period 1977-1995); b) fault-plane solutions from Gasparini *et al.* (1985) selected by Zoback (1992) for the World Stress Map (WSM) database (quality B and C).

University since 1977 (Pondrelli *et al.*, 1995) (fig. 2a). Recently published borehole breakout data (Amato *et al.*, 1995) confirm this active anti-Apenninic extension. From CMT solutions (fig. 2a), the northern margin of the Sicilian continental platform is characterized by a few thrust fault solutions which could be related to the south-verging thrusts in the sedimentary units of the northern portion of the island. In a previous study (Gasparini *et al.*, 1985) fault plane solutions of moderate and large events ($4.0 < M < 7.0$) which occurred in the Southern Apennines and Sicily in the period 1908-1980 were calculated. Figure 2b shows the best solutions of Gasparini *et al.* (1985) selected by Zoback (1992) for the World Stress Map (WSM) database (quality B and C). These solutions are mostly strike-slip and normal faults, except for a few (two north of Sicily and one in the Adriatic Sea). *T*-axes generally are NE-SW in the Southern Apennines, while in the Calabrian arc and in Sicily they are more scattered.

This work focuses on the distribution of different strain domains in Southern Italy as inferred from an analysis of new fault plane solutions of small ($M < 4.5$) recent earthquakes. The availability of digital data from the national seismic network (RSNC) of the Istituto Nazionale di Geofisica (ING) (fig. 3) since 1988 has allowed us to conduct a systematic investigation of the seismicity of the Southern Apennines and Sicilian region. This is the third part of a study of fault plane solutions in the entire Italian peninsula (Frepoli *et al.*, 1996; Frepoli and Amato, 1997). The results of the focal mechanisms analysis for the entire peninsula were summarized by Montone *et al.* (1997) in a synthesis of data on the present-day stress field in Italy. Here, we describe the focal mechanism data in greater detail, showing the distribution of *P*- and *T*-axes and the stress regime in subregions of Central and Southern Italy, including Calabria and Sicily. In the paper by Montone *et al.* (1997), only the horizontal projections of *P* and *T* axes for all the focal mechanisms of the Italian data set (1988-1995) were shown, and compared with breakout inferred stress directions. In this paper, we describe the individual solutions of 173 earthquakes, both showing the polarity distribution on the focal sphere and reporting the hypocentral parameters and focal mechanism parameters, in order to allow the use and quality assessment of these data. After comparing these data with previously published focal mechanisms and *in situ* stress measurements (Amato *et al.*, 1995), we finally propose a regional subdivision of the active tectonic processes in this complex region of the Mediterranean.

2. Data selection

We analyzed more than 400 fault plane solutions of earthquakes that occurred in the Southern Apennines, Calabria and Sicily in the period 1988-1995 and were recorded by the RSNC. The selected events have magnitude M_d ranging from 2.5 to 4.4. From this data set we selected 173 fault plane solutions (fig. 4; table I) following the two output quality factors Q_f and Q_p of the code FPFIT (Reasenberg and Oppenheimer, 1985) ranging from A to C for decreasing quality (table II). Q_f reflects the solution prediction misfit of the polarity data F_j, while Q_p reflects the solution uniqueness in terms of 90% confidence regions on strike, dip and rake. Frepoli and Amato (1997) investigated the stability of several fault plane solutions belonging to the data set of the Northern Apennines, testing the influence of the hypocentral errors and the velocity model. The focal mechanisms computed in this study have similar data distribution and coverage as those of the Northern Apennines data set. The average number of polarities per event used in this study is 15, and the formal location errors in depth (ERZ in Hypoinverse) are 2 km on the average, similar to the values in Frepoli and Amato (1997). Also, the two data sets are affected by the same uncertainty on the velocity model. Therefore, we estimate that the distribution of fault plane solutions has the same reliability as that of our previous paper, at least in terms of *P* and *T* axes. Frepoli and Amato (1997) found that the selected focal mechanisms (for which A-A, A-B, B-A, and B-B quality were obtained) are relatively well constrained, and that the variations on trend and plunge of *P* and *T* axes do not vary significantly, although in some cases the nodal planes appear to be less constrained.

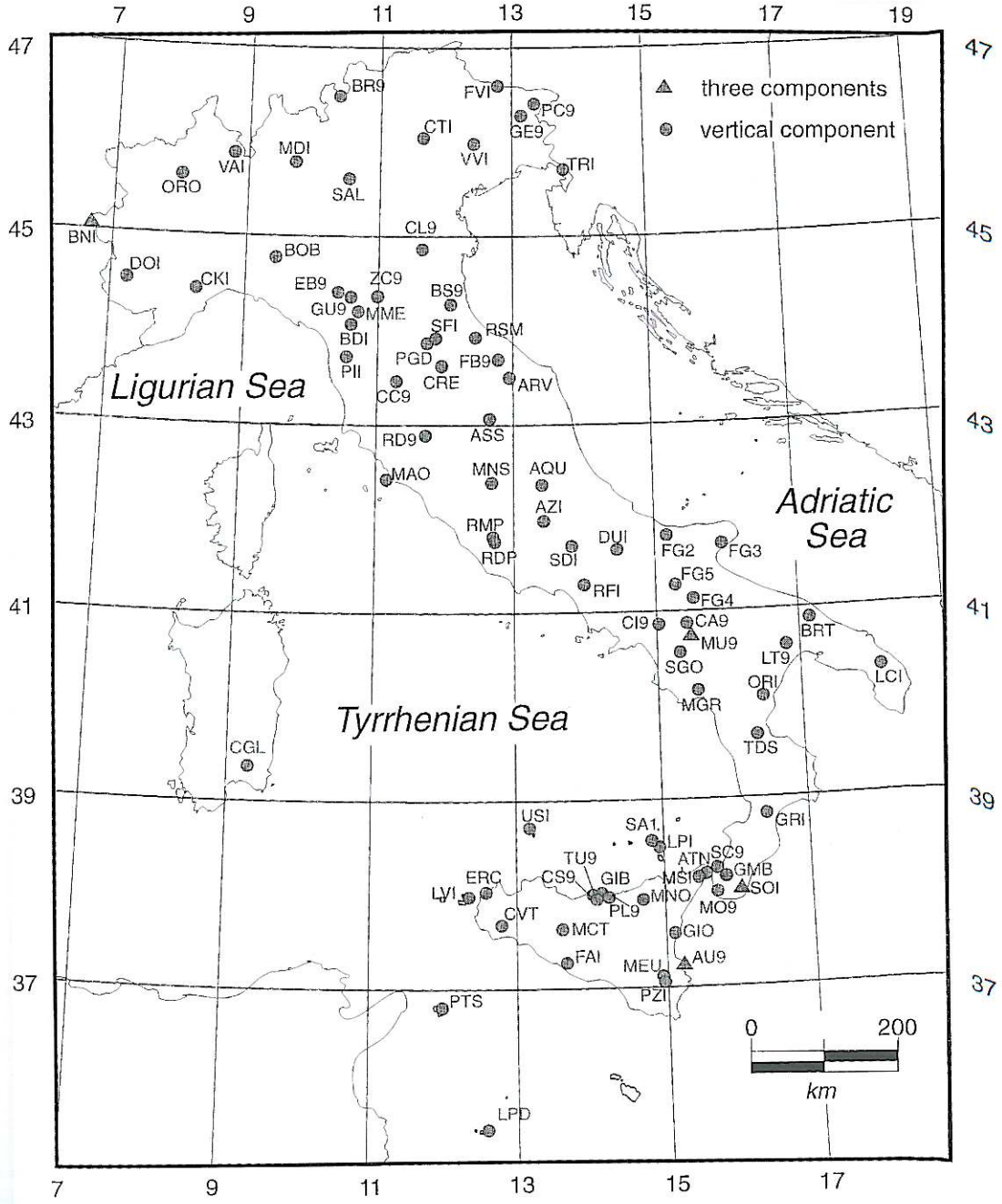

Fig. 3. Station distribution map of the national Italian seismic network (RSNC).

University since 1977 (Pondrelli *et al.*, 1995) (fig. 2a). Recently published borehole breakout data (Amato *et al.*, 1995) confirm this active anti-Apenninic extension. From CMT solutions (fig. 2a), the northern margin of the Sicilian continental platform is characterized by a few thrust fault solutions which could be related to the south-verging thrusts in the sedimentary units of the northern portion of the island. In a previous study (Gasparini *et al.*, 1985) fault plane solutions of moderate and large events ($4.0 < M < 7.0$) which occurred in the Southern Apennines and Sicily in the period 1908-1980 were calculated. Figure 2b shows the best solutions of Gasparini *et al.* (1985) selected by Zoback (1992) for the World Stress Map (WSM) database (quality B and C). These solutions are mostly strike-slip and normal faults, except for a few (two north of Sicily and one in the Adriatic Sea). *T*-axes generally are NE-SW in the Southern Apennines, while in the Calabrian arc and in Sicily they are more scattered.

This work focuses on the distribution of different strain domains in Southern Italy as inferred from an analysis of new fault plane solutions of small ($M < 4.5$) recent earthquakes. The availability of digital data from the national seismic network (RSNC) of the Istituto Nazionale di Geofisica (ING) (fig. 3) since 1988 has allowed us to conduct a systematic investigation of the seismicity of the Southern Apennines and Sicilian region. This is the third part of a study of fault plane solutions in the entire Italian peninsula (Frepoli *et al.*, 1996; Frepoli and Amato, 1997). The results of the focal mechanisms analysis for the entire peninsula were summarized by Montone *et al.* (1997) in a synthesis of data on the present-day stress field in Italy. Here, we describe the focal mechanism data in greater detail, showing the distribution of *P*- and *T*-axes and the stress regime in subregions of Central and Southern Italy, including Calabria and Sicily. In the paper by Montone *et al.* (1997), only the horizontal projections of *P* and *T* axes for all the focal mechanisms of the Italian data set (1988-1995) were shown, and compared with breakout inferred stress directions. In this paper, we describe the individual solutions of 173 earthquakes, both showing the polarity distribution on the focal sphere and reporting the hypocentral parameters and focal mechanism parameters, in order to allow the use and quality assessment of these data. After comparing these data with previously published focal mechanisms and *in situ* stress measurements (Amato *et al.*, 1995), we finally propose a regional subdivision of the active tectonic processes in this complex region of the Mediterranean.

2. Data selection

We analyzed more than 400 fault plane solutions of earthquakes that occurred in the Southern Apennines, Calabria and Sicily in the period 1988-1995 and were recorded by the RSNC. The selected events have magnitude M_d ranging from 2.5 to 4.4. From this data set we selected 173 fault plane solutions (fig. 4; table I) following the two output quality factors Q_f and Q_p of the code FPFIT (Reasenberg and Oppenheimer, 1985) ranging from A to C for decreasing quality (table II). Q_f reflects the solution prediction misfit of the polarity data F_j, while Q_p reflects the solution uniqueness in terms of 90% confidence regions on strike, dip and rake. Frepoli and Amato (1997) investigated the stability of several fault plane solutions belonging to the data set of the Northern Apennines, testing the influence of the hypocentral errors and the velocity model. The focal mechanisms computed in this study have similar data distribution and coverage as those of the Northern Apennines data set. The average number of polarities per event used in this study is 15, and the formal location errors in depth (ERZ in Hypoinverse) are 2 km on the average, similar to the values in Frepoli and Amato (1997). Also, the two data sets are affected by the same uncertainty on the velocity model. Therefore, we estimate that the distribution of fault plane solutions has the same reliability as that of our previous paper, at least in terms of *P* and *T* axes. Frepoli and Amato (1997) found that the selected focal mechanisms (for which A-A, A-B, B-A, and B-B quality were obtained) are relatively well constrained, and that the variations on trend and plunge of *P* and *T* axes do not vary significantly, although in some cases the nodal planes appear to be less constrained.

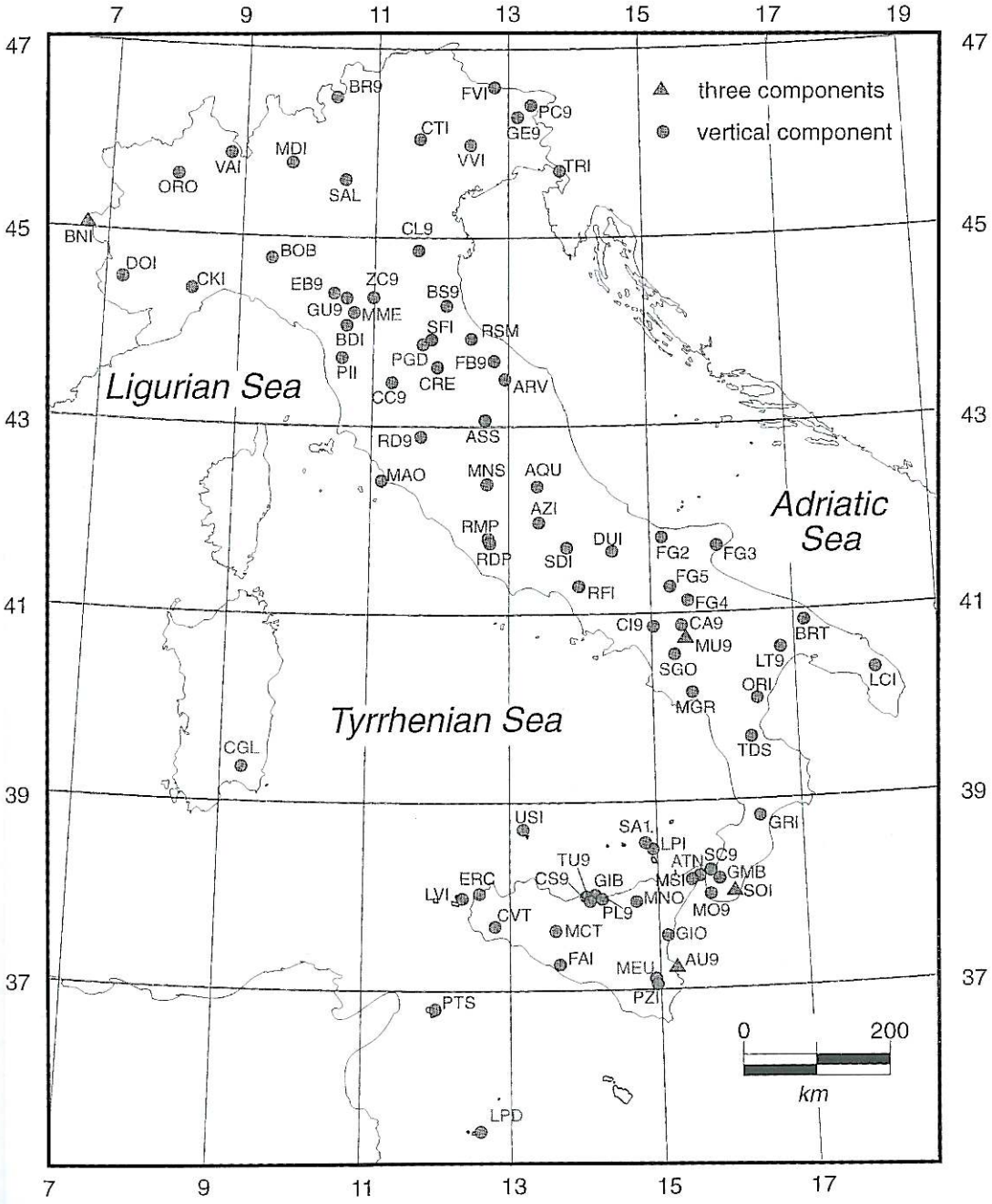

Fig. 3. Station distribution map of the national Italian seismic network (RSNC).

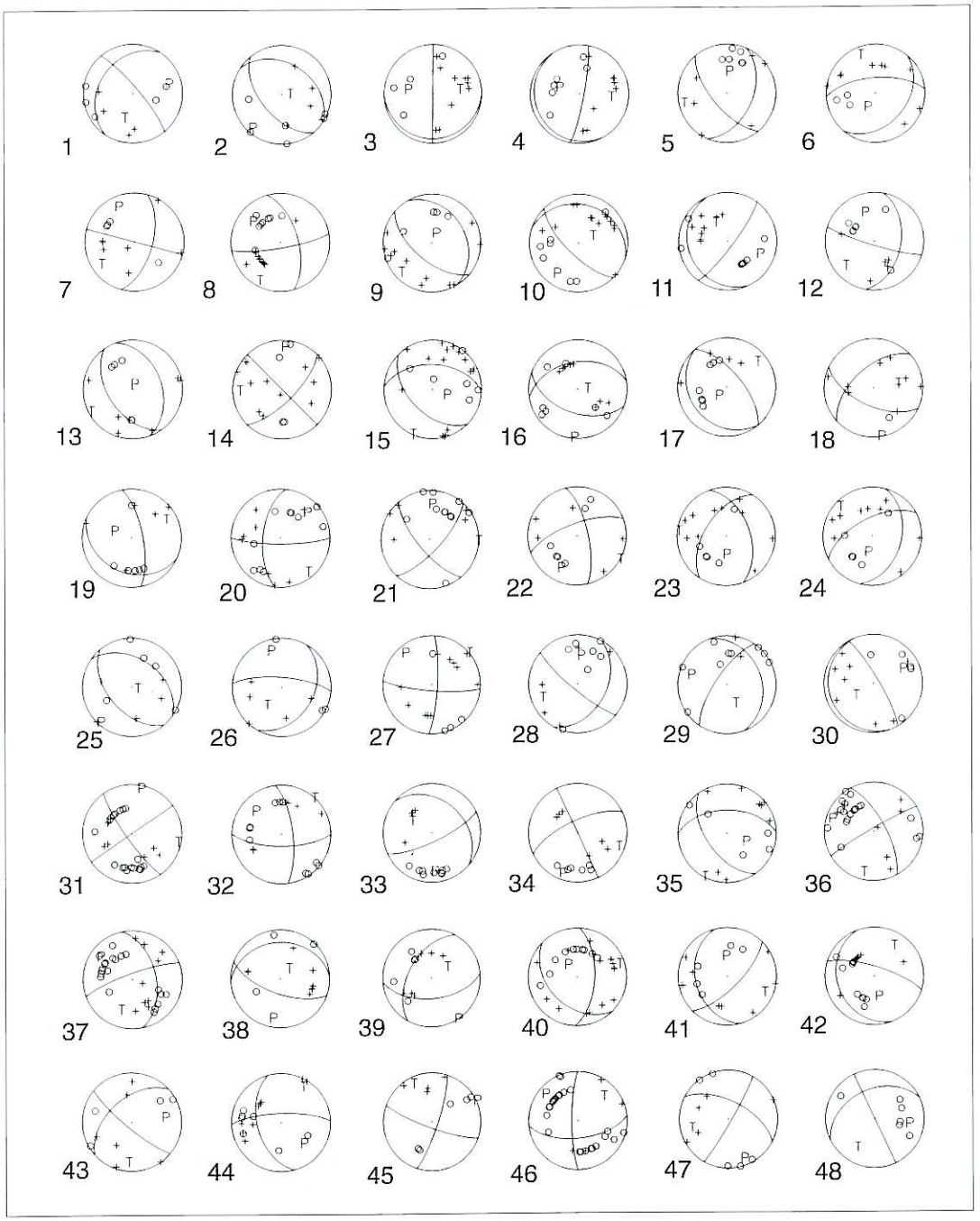

Fig. 4. Schmidt lower hemisphere projection of the 173 selected fault-plane solutions of this study. Compression and dilatation polarities are indicated with crosses and circles, respectively.

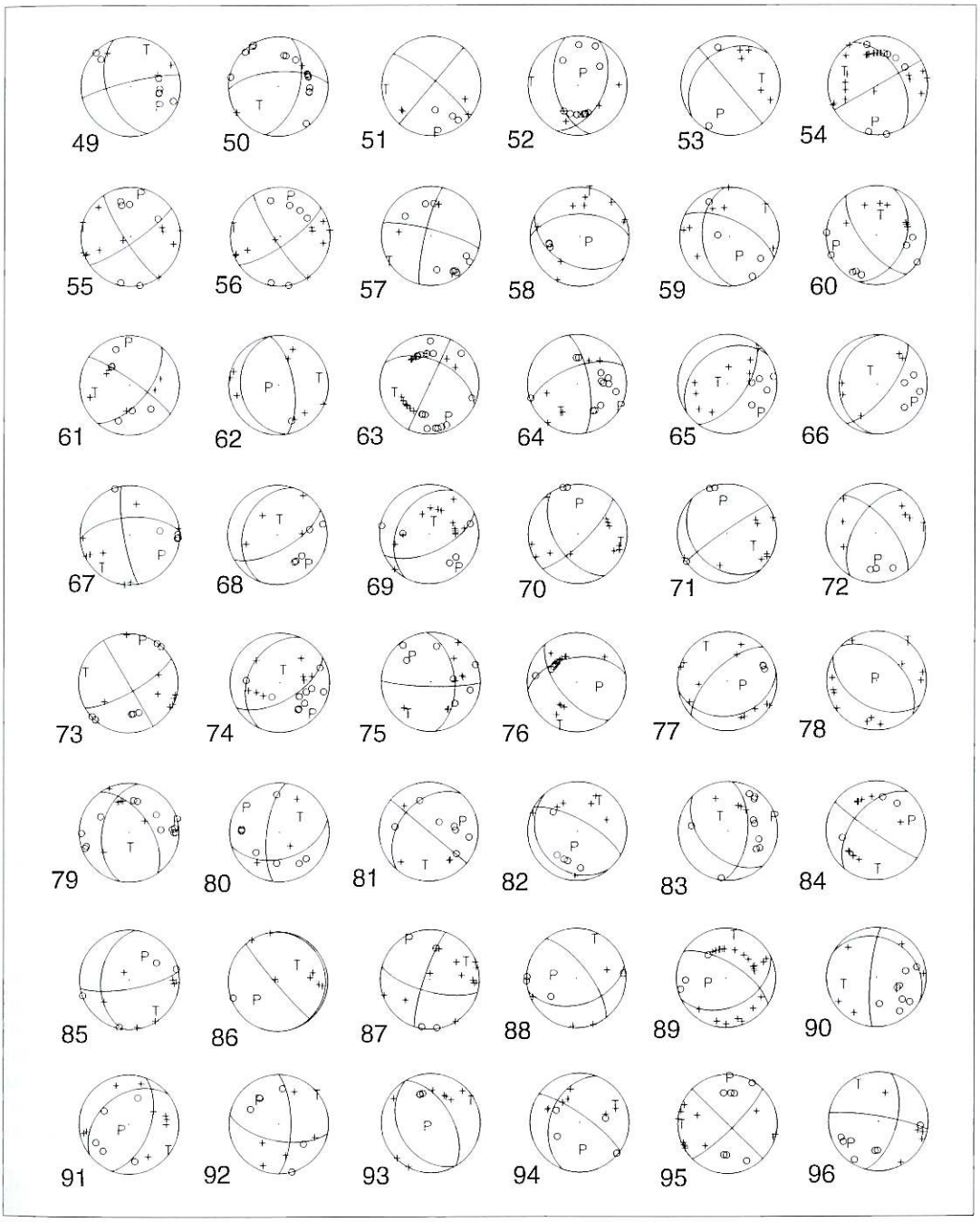

Fig. 4 (*continued*).

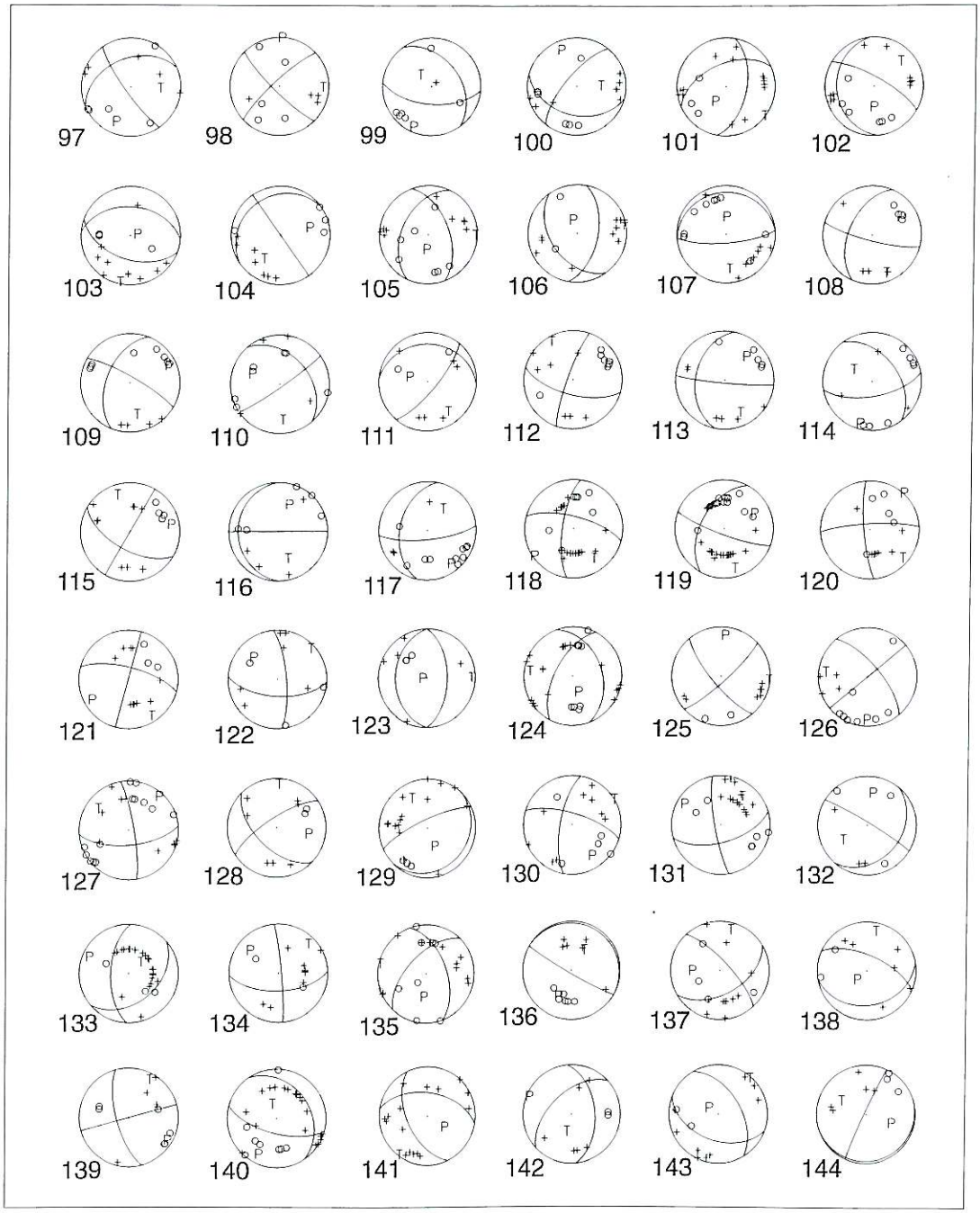

Fig. 4 (*continued*).

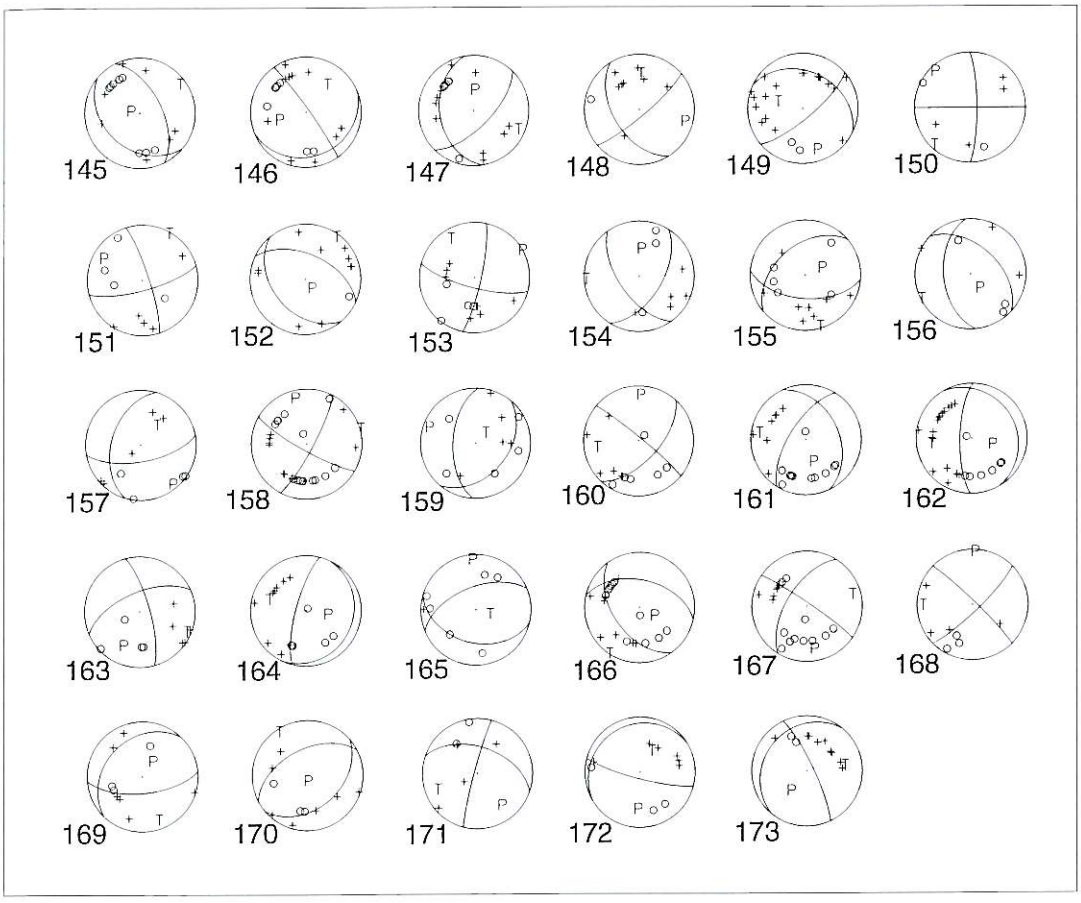

Fig. 4 (*continued*).

We used plunges of *P*- and *T*-axes to divide our data set into five main stress regime categories (tables III and IV) following Zoback (1992) for the WSM. An additional category is considered (unknown category) when the plunges of axes fall outside the ranges defined in the table (see also Frepoli and Amato, 1997 and Montone *et al.*, 1997).

In this paper, we describe and discuss only the distributions of *T* and *P* axes, trying to identify qualitatively the areas which show internal consistence, both in terms of type of faulting (normal, strike-slip, or thrust faulting) and of mean direction of extension and compression. For this reason, we do not discuss the solutions (22 out of 173) belonging to the category «U» (unknown stress regime), that is, those with strongly oblique *P* and *T* axes.

3. Results

As in Frepoli and Amato (1997) we grouped focal mechanisms in different geographic sectors following both the distribution of event clusters and of fault-plane solution categories (fig. 5). Figures 6a-d and 7a-d plot the *P*- and *T*-axes of the different focal mechanism catego-

Table I. Hypocentral parameters, magnitudes, location azimuthal gaps, location errors and geographic sector indications of the 173 events with selected fault-plane solutions.

No.	Date	Orig. time	Lat.	Long.	Z	Gap	M_d	RMS	ERH	ERZ	Area
1	880813	12:50	37 53	14 54	26.9	159	3.4	0.20	4.3	1.5	Nebrodi Mt.
2	880816	23:46	38 32	14 37	16.4	164	3.2	0.28	1.6	1.5	Aeolie Islands
3	890624	02:34	37 54	14 45	7.4	87	3.3	0.10	0.9	0.6	Nebrodi Mt.
4	890624	05:49	37 54	14 44	7.6	86	3.4	0.16	1.0	0.9	Nebrodi Mt.
5	891110	03:19	37 36	15 01	27.6	202	3.4	0.10	1.2	1.0	Etna
6	891121	18:36	38 07	15 54	10.4	204	3.8	0.27	2.0	1.3	Southern Calabria
7	891125	18:21	41 41	15 55	18.6	124	3.5	0.30	2.4	1.6	Gargano
8	900124	04:45	39 07	16 59	7.0	180	2.9	0.21	1.0	2.5	Southern Apennines
9	900218	00:28	38 06	15 09	17.3	88	3.1	0.18	0.6	1.9	Aeolie Islands
10	900316	09:52	37 44	14 59	9.4	179	3.5	0.22	1.3	4.2	Etna
11	900416	19:09	41 45	14 14	7.8	132	3.4	0.33	1.5	2.2	Central Apennines
12	900503	04:57	41 09	14 52	1.7	132	3.4	0.24	1.1	4.0	Southern Apennines
13	900505	08:58	40 38	15 46	14.1	96	3.6	0.21	0.9	3.2	Southern Apennines
14	901005	17:58	38 32	14 49	22.9	198	3.4	0.49	6.1	1.9	Aeolie Islands
15	901216	13:50	37 16	15 15	16.3	147	3.8	0.42	1.1	1.7	Southern Sicily
16	910126	01:26	41 03	13 18	3.9	118	3.6	0.16	2.9	5.9	Central Apennines
17	910615	20:58	38 47	16 54	8.5	238	4.0	0.20	2.9	2.8	Southern Apennines
18	910714	17:51	37 56	14 22	4.5	116	3.2	0.34	1.2	2.6	Nebrodi Mt.
19	910906	15:59	39 03	15 34	25.4	123	3.2	0.19	1.0	1.7	Aeolie Islands
20	910907	05:39	37 58	15 31	8.3	124	3.5	0.17	0.6	1.8	Southern Calabria
21	910920	19:54	37 34	14 52	15.7	119	3.5	0.29	0.9	2.4	Etna
22	910925	13:21	37 59	16 01	9.9	199	3.3	0.29	1.5	1.6	Southern Calabria
23	910925	14:53	37 59	16 02	10.4	203	3.5	0.35	1.4	1.6	Southern Calabria
24	910925	21:21	37 59	16 01	8.9	202	3.4	0.34	1.4	1.6	Southern Calabria
25	910927	20:10	38 30	14 40	17.6	157	3.3	0.26	1.8	1.2	Aeolie Islands
26	910927	20:13	38 31	14 36	17.3	162	3.3	0.21	1.5	1.0	Aeolie Islands
27	911003	02:40	38 50	15 14	15.5	133	3.7	0.35	1.1	2.3	Aeolie Islands
28	911023	21:36	37 40	15 12	29.6	131	3.5	0.30	2.3	1.8	Etna
29	911214	09:54	37 40	15 04	18.5	102	3.5	0.19	0.9	1.6	Etna
30	911214	18:41	37 44	14 54	11.5	105	3.5	0.27	0.8	2.3	Etna
31	920218	03:30	42 19	14 16	5.0	186	3.8	0.31	2.1	–	Central Apennines
32	920228	18:33	37 40	16 14	22.3	235	3.4	0.25	4.0	2.0	Southern Calabria
33	920229	04:04	42 13	14 17	10.0	159	3.2	0.37	2.0	–	Central Apennines
34	920315	03:15	42 11	14 13	5.0	145	2.9	0.35	1.9	–	Central Apennines
35	920316	05:45	41 23	14 01	7.8	164	3.4	0.25	0.9	1.9	Central Apennines
36	920318	16:29	41 14	14 49	12.2	88	3.6	0.38	0.8	1.0	Southern Apennines
37	920319	23:34	41 30	14 36	13.5	82	3.5	0.26	0.6	0.4	Southern Apennines
38	920328	10:21	38 28	14 36	26.3	162	3.3	0.26	1.5	0.7	Aeolie Islands
39	920401	07:25	38 52	17 06	3.5	198	3.3	0.34	1.9	4.6	Southern Apennines
40	920406	13:08	37 49	14 37	8.7	123	3.8	0.36	1.2	2.4	Nebrodi Mt.
41	920503	01:30	38 11	15 13	17.0	108	3.0	0.27	2.1	1.3	Aeolie Islands
42	920530	21:40	39 54	16 52	2.5	133	3.5	0.23	0.8	4.0	Southern Apennines
43	920613	09:32	38 20	15 50	9.0	116	3.2	0.29	1.0	1.3	Southern Calabria
44	920617	05:41	41 24	15 42	10.4	104	3.4	0.43	1.5	2.9	Gargano

Table I (*continued*).

No.	Date	Orig. time	Lat.	Long.	Z	Gap	M_d	RMS	ERH	ERZ	Area
45	920628	06:03	38 20	15 48	14.2	98	3.3	0.24	0.9	1.1	Southern Calabria
46	920716	05:38	42 11	14 11	18.9	145	4.0	0.30	1.7	1.5	Central Apennines
47	920731	22:29	37 32	16 02	18.4	240	2.6	0.36	3.6	2.6	Southern Calabria
48	920805	21:35	37 29	13 10	1.1	118	3.2	0.06	0.7	1.5	NW Sicily
49	920806	03:06	37 25	13 08	10.8	203	3.3	0.21	1.5	1.8	NW Sicily
50	920806	04:23	37 22	13 06	16.1	137	3.6	0.33	1.2	2.4	NW Sicily
51	920826	03:40	37 53	16 06	32.3	237	2.9	0.28	3.2	3.2	Southern Calabria
52	920828	13:05	39 39	15 17	11.5	151	4.1	0.10	0.7	2.3	Policastro Gulf
53	920903	10:38	37 02	15 05	10.7	251	3.1	0.21	3.5	1.6	Southern Sicily
54	920927	11:55	37 54	14 40	23.3	120	3.7	0.31	1.4	1.2	Nebrodi Mt.
55	920927	12:19	37 55	14 39	23.6	119	3.3	0.35	1.6	1.2	Nebrodi Mt.
56	920927	22:40	37 55	14 40	23.4	117	3.3	0.33	1.6	1.3	Nebrodi Mt.
57	921111	10:43	37 49	16 07	22.5	287	3.3	0.18	5.5	2.2	Southern Calabria
58	921220	21:48	38 21	16 06	17.5	161	3.2	0.09	0.8	2.0	Southern Calabria
59	930101	18:46	41 37	13 59	10.7	103	3.2	0.24	0.9	1.1	Central Apennines
60	930317	00:07	37 38	13 52	19.8	149	3.4	0.42	1.9	2.2	NW Sicily
61	930405	22:55	40 40	15 45	1.1	70	3.5	0.35	0.7	0.4	Southern Apennines
62	930410	03:46	37 53	14 28	9.0	119	2.9	0.09	0.5	1.0	Nebrodi Mt.
63	930509	01:28	39 03	15 31	13.8	126	3.5	0.38	1.5	4.4	Aeolie Islands
64	930510	18:30	38 01	14 09	1.0	133	3.5	0.24	0.8	–	NW Sicily
65	930514	21:25	38 00	14 09	2.0	132	2.9	0.30	1.0	0.7	NW Sicily
66	930521	19:01	38 01	14 08	6.0	132	3.2	0.32	1.3	2.5	NW Sicily
67	930524	11:50	37 58	14 56	20.9	150	3.1	0.29	3.1	1.4	Nebrodi Mt.
68	930602	20:04	38 01	14 08	2.0	171	2.8	0.26	1.4	–	NW Sicily
69	930626	17:47	38 01	14 08	2.9	148	4.4	0.17	0.6	0.9	NW Sicily
70	930701	20:41	37 49	14 38	22.7	158	3.0	0.18	2.4	0.9	Nebrodi Mt.
71	930701	21:23	37 43	14 38	20.7	132	2.8	0.10	0.5	1.0	Nebrodi Mt.
72	930703	03:36	37 44	14 56	4.4	87	2.8	0.32	0.8	2.5	Etna
73	930709	15:51	38 28	14 41	17.4	204	3.2	0.25	2.0	1.3	Aeolie Islands
74	930728	21:28	37 58	14 10	2.5	104	3.2	0.24	0.8	0.4	NW Sicily
75	930730	18:40	38 02	14 09	2.0	93	3.1	0.30	0.8	1.4	NW Sicily
76	930810	01:14	39 35	17 01	8.6	159	3.9	0.33	1.4	4.0	Southern Apennines
77	930811	14:46	37 50	14 29	10.0	128	3.2	0.09	0.4	1.3	Nebrodi Mt.
78	930824	01:20	38 11	15 08	13.3	88	2.9	0.19	0.9	1.5	Aeolie Islands
79	931012	20:21	38 00	14 49	22.9	143	3.6	0.26	2.0	1.1	Nebrodi Mt.
80	931018	07:25	37 54	15 48	31.8	223	2.9	0.26	3.8	2.1	Southern Calabria
81	940223	08:33	38 00	14 03	6.2	142	3.3	0.31	2.2	1.1	NW Sicily
82	940223	23:57	39 52	16 28	15.5	114	3.4	0.30	1.3	1.1	Southern Apennines
83	940228	20:43	37 35	13 43	7.2	185	3.2	0.37	2.1	3.2	NW Sicily
84	940326	13:25	38 53	16 39	26.7	217	3.4	0.18	3.0	0.8	Southern Apennines
85	940421	15:07	37 58	14 40	18.4	97	2.9	0.25	1.5	1.4	Nebrodi Mt.
86	940421	17:05	37 57	14 41	22.0	144	2.6	0.14	1.8	0.7	Nebrodi Mt
87	940421	19:28	37 57	14 42	19.3	96	3.0	0.27	1.4	1.0	Nebrodi Mt.

Table I (*continued*).

No.	Date	Orig. time	Lat.	Long.	Z	Gap	M_d	RMS	ERH	ERZ	Area
88	940504	14:13	37 59	14 54	17.1	147	2.8	0.22	2.0	1.3	Nebrodi Mt.
89	940506	19:09	37 44	14 08	11.1	143	3.8	0.23	1.3	2.0	NW Sicily
90	940601	02:43	37 54	14 09	11.9	91	2.8	0.39	1.4	1.9	NW Sicily
91	940608	23:49	38 05	14 38	8.4	82	2.8	0.32	0.9	2.1	Nebrodi Mt.
92	940611	04:09	40 46	15 20	17.9	124	3.4	0.31	1.9	1.6	Southern Apennines
93	940621	05:56	36 47	14 37	13.9	259	3.0	0.28	2.2	1.6	Southern Sicily
94	940621	09:01	41 27	13 44	5.0	162	3.3	0.21	1.1	–	Central Apennines
95	940707	14:03	38 19	15 00	16.1	86	3.6	0.15	0.6	1.1	Aeolie Islands
96	940708	05:36	38 19	15 00	10.8	85	3.0	0.13	0.8	2.0	Aeolie Islands
97	940714	02:42	38 20	14 59	15.6	86	2.7	0.33	1.2	2.9	Aeolie Islands
98	940714	03:18	38 19	15 00	2.7	131	2.5	0.19	0.8	2.9	Aeolie Islands
99	940717	11:18	37 39	13 40	25.8	172	2.7	0.22	4.9	3.1	NW Sicily
100	940723	20:57	38 08	15 11	10.5	106	2.7	0.22	0.7	2.9	Aeolie Islands
101	940808	17:38	38 02	14 39	9.6	108	3.3	0.23	1.2	7.8	Nebrodi Mt.
102	940808	19:48	38 05	14 39	7.3	118	3.4	0.31	0.9	2.5	Nebrodi Mt.
103	940819	01:51	37 57	15 49	15.9	158	3.0	0.20	1.0	1.5	Southern Calabria
104	940823	20:00	38 02	15 19	13.1	144	2.8	0.20	1.5	2.5	Southern Calabria
105	940908	02:39	37 56	14 39	9.4	100	3.2	0.21	0.6	0.9	Nebrodi Mt.
106	940910	13:19	38 06	15 07	6.7	96	2.7	0.26	1.3	2.8	Aeolie Islands
107	940920	19:10	41 49	13 47	6.6	95	3.5	0.23	0.9	1.5	Central Apennines
108	940926	19:28	37 40	15 00	3.6	99	2.5	0.29	0.8	3.7	Etna
109	940926	19:38	37 41	14 59	12.7	98	3.1	0.17	0.5	3.5	Etna
110	940926	19:43	37 49	14 58	20.0	170	3.1	0.23	1.6	1.5	Etna
111	940926	21:08	37 40	15 00	2.3	99	2.5	0.35	1.1	5.5	Etna
112	940926	21:20	37 46	15 00	7.6	175	2.7	0.21	1.2	3.0	Etna
113	940926	21:49	37 46	15 00	9.7	216	2.6	0.17	1.8	2.7	Etna
114	940926	22:48	37 46	14 59	13.9	176	2.7	0.24	3.3	4.8	Etna
115	940927	00:26	37 45	15 00	4.4	178	2.9	0.23	2.3	3.7	Etna
116	940929	04:25	37 56	15 32	11.0	131	2.8	0.27	0.9	1.5	Southern Calabria
117	941001	22:37	38 29	15 06	11.2	75	3.2	0.22	0.8	1.5	Aeolie Islands
118	941011	16:35	39 43	15 19	1.2	140	3.6	0.26	1.0	0.2	Policastro Gulf
119	941012	04:59	39 42	15 19	0.7	89	3.9	0.35	0.9	0.2	Policastro Gulf
120	941016	21:52	39 41	15 19	1.3	150	3.2	0.17	0.7	0.2	Policastro Gulf
121	941019	11:09	39 42	15 17	1.2	176	3.2	0.38	2.1	0.5	Policastro Gulf
122	941020	13:25	37 52	14 59	24.5	88	2.7	0.34	0.7	2.2	Etna
123	941112	21:35	40 26	15 44	8.4	86	3.5	0.31	1.0	3.4	Southern Apennines
124	941127	07:26	38 23	14 53	16.3	109	3.7	0.21	0.6	1.1	Aeolie Islands
125	941127	07:30	38 22	14 54	12.2	115	2.9	0.15	1.4	3.9	Aeolie Islands
126	941211	18:22	37 56	15 37	15.0	178	2.9	0.36	1.9	2.2	Southern Calabria
127	950210	08:15	37 47	14 58	20.5	173	3.7	0.17	1.5	1.6	Etna
128	950211	02:12	37 41	15 01	1.4	95	2.9	0.32	0.8	1.6	Etna
129	950308	08:55	37 52	15 33	11.5	142	3.7	0.26	1.3	2.3	Southern Calabria
130	950405	20:29	37 40	13 55	20.2	96	3.4	0.23	0.9	1.1	NW Sicily

Table I (*continued*).

No.	Date	Orig. time	Lat.	Long.	Z	Gap	M_d	RMS	ERH	ERZ	Area
131	950411	12:06	37 35	13 59	8.7	154	3.8	0.44	1.6	4.6	NW Sicily
132	950517	15:47	37 41	14 59	6.2	225	2.7	0.39	3.9	8.3	Etna
133	950529	06:52	38 17	12 30	2.0	277	4.3	0.58	6.9	–	NW Sicily
134	950531	00:21	37 55	12 17	6.1	193	3.5	0.13	2.7	1.7	NW Sicily
135	950605	22:26	37 53	14 38	21.6	173	3.5	0.37	2.2	1.3	Nebrodi Mt.
136	950607	03:49	39 02	15 56	1.4	104	2.8	0.25	0.9	0.3	Southern Apennines
137	950613	07:37	40 42	15 21	18.0	110	3.3	0.37	1.4	1.4	Southern Apennines
138	950613	16:00	40 12	16 02	8.4	69	3.3	0.41	1.1	3.5	Southern Apennines
139	950627	01:44	37 38	13 58	14.0	88	3.0	0.35	1.0	2.4	NW Sicily
140	950723	18:44	38 32	14 43	17.5	151	4.4	0.18	1.0	0.7	Aeolie Islands
141	950724	16:58	37 59	15 24	11.4	156	3.7	0.31	1.0	1.8	Southern Calabria
142	950725	23:01	38 02	14 46	7.5	99	3.0	0.21	0.8	1.7	Nebrodi Mt.
143	950726	03:18	37 54	15 22	12.3	120	3.3	0.24	0.8	3.2	Southern Calabria
144	950803	12:15	37 48	15 33	3.5	151	2.9	0.30	1.0	4.3	Southern Calabria
145	950806	22:12	41 35	15 19	24.1	222	3.4	0.26	4.1	1.5	Gargano
146	950807	01:02	41 33	15 17	23.4	260	3.2	0.11	4.7	1.3	Gargano
147	950807	01:23	41 31	15 17	22.6	250	3.3	0.19	4.7	1.7	Gargano
148	950815	01:05	39 34	16 52	7.6	205	3.2	0.38	3.8	7.4	Southern Apennines
149	950827	19:42	38 16	15 17	18.4	96	4.0	0.23	1.4	1.2	Aeolie Islands
150	950830	21:11	37 49	14 59	4.3	170	2.5	0.15	1.8	2.5	Etna
151	950830	23:52	41 28	15 25	4.1	213	3.1	0.39	4.2	4.3	Gargano
152	950918	21:00	37 51	14 58	12.5	166	2.8	0.22	1.4	2.8	Etna
153	950918	21:05	41 59	15 21	4.3	232	3.1	0.19	1.6	1.3	Gargano
154	950919	05:30	40 37	15 47	23.4	109	3.1	0.34	1.2	2.5	Southern Apennines
155	950920	16:24	41 56	15 18	12.2	228	3.2	0.48	7.8	2.6	Gargano
156	950924	22:59	40 33	15 48	18.3	71	3.3	0.42	1.9	2.8	Southern Apennines
157	950924	23:43	38 32	14 48	15.5	152	2.9	0.31	1.2	0.9	Aeolie Islands
158	950930	10:14	41 45	15 56	22.0	181	4.4	0.40	1.4	0.6	Gargano
159	951003	05:30	38 02	14 06	2.0	93	3.1	0.40	1.1	–	NW Sicily
160	951003	20:40	41 44	15 59	23.4	224	3.0	0.15	3.8	1.7	Gargano
161	951004	02:00	41 45	15 57	23.2	203	3.2	0.23	2.4	0.9	Gargano
162	951005	23:51	41 43	15 55	21.9	183	3.6	0.36	2.3	1.1	Gargano
163	951014	03:41	38 32	14 46	16.3	154	2.8	0.27	1.5	0.9	Aeolie Islands
164	951022	07:33	41 43	15 57	20.8	223	3.1	0.26	3.3	1.5	Gargano
165	951104	14:16	38 11	14 54	24.6	97	2.6	0.16	0.6	1.0	Aeolie Islands
166	951108	09:45	41 41	15 57	18.1	134	3.4	0.30	4.7	2.7	Gargano
167	951108	14:20	41 40	15 56	16.6	123	3.4	0.34	3.7	2.5	Gargano
168	951120	05:44	41 35	15 52	14.2	151	2.8	0.24	3.0	2.9	Gargano
169	951202	17:19	39 34	16 43	10.2	184	3.4	0.26	1.2	2.3	Southern Apennines
170	951208	16:21	41 40	15 44	18.4	149	3.1	0.30	1.1	2.1	Gargano
171	951223	15:41	37 02	14 53	15.3	243	2.9	0.47	5.8	2.1	Southern Sicily
172	951224	01:31	37 54	14 36	6.5	149	2.9	0.30	1.8	3.1	Nebrodi Mt.
173	951228	22:11	37 01	13 59	0.4	230	3.6	0.23	2.9	0.4	Southern Sicily

Table II. Fault plane solution quality factors Q_f and Q_p (as described in Reasenberg and Oppenheimer, 1985). F_j is the solution prediction misfit to the polarity data. Δs, Δd and Δr are ranges of variability of strike of the dip, dip and rake, respectively.

	Q_f		Q_p
A	$F_j \leq 0.025$	A	Δstr, Δdip, Δrake $\leq 20°$
B	$0.025 < F_j \leq 0.1$	B	20° to 40°
C	$F_j > 0.1$	C	> 40°

Table III. Fault plane solution categories based on different plunge ranges for *P*- and *T*-axes according to Zoback (1992) for the WSM.

Plunge of axes		F.P.S. categories
P	*T*	
pl ≥ 52°	pl ≤ 35°	NF
40° ≤ pl < 52°	pl ≤ 20°	NS
pl < 40°	pl ≤ 20°	SS
pl ≤ 20°	pl < 40°	SS
pl ≤ 20°	40° ≤ pl < 52°	TS
pl ≤ 35°	pl ≥ 52°	TF

ries. In these plots categories NS-NF (normal-strike and normal), and TS-TF (thrust-strike and thrust) are grouped together. The *P*- and *T*-axes of the unknown category (U) are not plotted.

3.1. *Central Apennines sector*

In the Central Apennines we selected ten events with well constrained fault plane solutions: four are NF, three are SS and three are TF. Magnitudes range between 2.9 and 4.0, and hypocentral depths are in the upper 20 km. The NF solutions are concentrated in the south-western portion of this sector. Three of these solutions have *T*-axes NE-SW oriented while one is N-S. The SS are grouped along the Adriatic coast. Two of them have *T*-axes ESE-WNW oriented and one NE-SW. The TF solutions are scattered in a large area with *T*-axes of two solutions N-S and one NW-SE oriented.

3.2. *Southern Apennines sector*

This sector is characterized by evident NE-SW extension. There are six NF, four SS and one U solution. Generally *T*-axes of both category solutions are NE-SW. The two SS solutions of the Sannio-Matese area have *T*-axes NNE-SSW as the two NF solutions of the Val d'Agri and the Northern Irpinia areas, respectively. Two NF solutions in the Irpinia area have *T*-axes E-W while two NF and two SS in the same area have *T*-axes NE-SW. Hypocentral depths are in the upper 23 km and magnitudes range between 3.1 and 3.6.

3.3. *Gargano sector*

In this portion of Southern Italy we selected 17 focal mechanisms of which nine are NF, seven are SS and one is a U solution. Events which

Table IV. Fault plane solution parameters of the analyzed events. The table reports event number, date, origin time, strike of the dip, dip and rake (the first nodal plane dipping to the east going clockwise from the north is reported), azimuth and plunge of *P*- and *T*-axes, fault-plane solution category, number of polarities and quality factor for the 173 selected focal mechanisms.

No.	Date	Orig. time	Strike	Dip	Rake	*P* azim.	Axes plun.	*T* azim.	Axes plun.	F.P.S. classes	Pol. num.	Q_f	Q_p
1	880813	12:50	50	80	60	73	28	199	46	U	9	A	A
2	880816	23:46	230	55	100	222	9	84	77	TF	11	A	A
3	890624	02:34	180	10	−180	279	44	80	44	U	14	B	A
4	890624	05:49	240	10	−130	287	52	94	37	U(NF)	14	A	A
5	891110	03:19	230	65	−130	2	52	257	11	NF	13	A	A
6	891121	18:36	130	35	−130	215	62	338	15	NF	12	A	A
7	891125	18:21	105	60	0	334	20	235	20	SS	11	A	A
8	900124	04:45	170	80	−150	306	28	208	13	SS	20	A	B
9	900218	00:28	220	60	−100	15	73	227	14	NF	16	A	A
10	900316	09:52	225	70	100	217	24	61	63	TF	21	B	A
11	900416	19:09	245	20	30	111	32	326	51	U(TF)	16	A	B
12	900503	04:57	100	45	−10	339	35	230	24	U	12	A	A
13	900505	08:58	235	50	−100	2	81	242	4	NF	12	A	B
14	901005	17:58	135	70	0	1	13	268	13	SS	16	B	A
15	901216	13:50	225	50	−60	112	67	204	0	NF	23	B	A
16	910126	01:26	200	50	110	185	3	84	74	TF	15	B	B
17	910615	20:58	230	25	−90	230	70	50	20	NF	12	A	A
18	910714	17:51	205	60	140	172	2	79	48	TS	10	A	A
19	910906	15:59	205	30	−140	290	57	60	22	NF	11	B	A
20	910907	05:39	180	80	−30	43	28	141	13	SS	19	B	A
21	910920	19:54	230	70	−160	1	27	91	0	SS	16	B	A
22	910925	13:21	340	70	−20	208	27	118	0	SS	11	A	A
23	910925	14:53	70	50	−130	183	60	277	20	NF	15	A	A
24	910925	21:21	105	40	−130	199	62	312	11	NF	14	A	A
25	910927	20:10	230	50	100	222	4	102	81	TF	11	B	A
26	910927	20:13	120	35	30	341	22	220	51	U(TF)	8	A	A
27	911003	02:40	185	80	−170	319	14	49	0	SS	16	A	A
28	911023	21:36	220	80	−130	2	41	249	24	U	13	B	A
29	911214	09:54	70	30	40	285	22	155	57	TF	11	A	A
30	911214	18:41	250	10	100	61	35	237	54	TF	13	B	A
31	920218	03:30	235	80	−180	9	7	100	7	SS	29	B	A
32	920228	18:33	180	70	−160	311	27	41	0	SS	19	A	A
33	920229	04:04	155	75	60	177	24	301	50	U(TF)	13	A	B
34	920315	03:15	65	90	−160	201	13	108	13	SS	12	A	A
35	920316	05:45	235	55	−50	114	58	207	2	NF	13	A	A
36	920318	16:29	240	85	160	287	10	194	17	SS	29	A	A
37	920319	23:34	250	80	140	300	17	207	10	SS	33	A	A
38	920328	10:21	200	65	100	192	19	39	68	TF	11	A	A
39	920401	07:25	175	55	130	147	2	54	58	TF	14	A	A
40	920406	13:08	225	40	−130	319	62	72	11	NF	28	B	A
41	920503	01:30	135	70	−60	352	54	112	19	NF	14	A	A
42	920530	21:40	250	25	−40	171	56	32	26	NF	20	A	A

Table IV (*continued*).

No.	Date	Orig. time	Strike	Dip	Rake	P azim.	Axes plun.	T azim.	Axes plun.	F.P.S. classes	Pol. num.	Q_f	Q_p
43	920613	09:32	220	80	−40	81	34	185	18	SS	11	B	A
44	920617	05:41	255	50	−20	134	39	31	15	U(NS)	17	B	A
45	920628	06:03	200	80	10	64	0	334	14	SS	9	A	A
46	920716	05:38	270	80	30	308	13	46	28	SS	33	B	A
47	920731	22:29	120	85	30	159	16	257	24	SS	10	A	B
48	920805	21:35	65	90	50	97	32	212	32	U	6	A	B
49	920806	03:06	250	50	−10	126	33	21	21	U(SS)	11	A	B
50	920806	04:23	105	55	30	323	6	226	44	TS	20	B	A
51	920826	03:40	130	90	10	174	7	265	7	SS	9	A	A
52	920828	13:05	115	45	−60	14	68	274	3	NF	17	A	A
53	920903	10:38	50	90	−120	203	37	76	37	U	7	A	B
54	920927	11:55	150	90	40	187	27	292	27	U	37	B	A
55	920927	12:19	145	80	−10	10	14	280	0	SS	19	A	A
56	920927	22:40	145	75	−10	11	17	280	3	SS	18	A	A
57	921111	10:43	15	80	−170	149	14	239	0	SS	11	A	B
58	921220	21:48	205	40	−70	127	75	10	6	NF	12	A	A
59	930101	18:46	265	45	−40	156	55	51	10	NF	11	A	A
60	930317	00:07	110	40	140	255	14	8	56	TF	18	B	B
61	930405	22:55	130	60	10	355	14	258	27	SS	14	A	A
62	930410	03:46	80	65	−90	260	70	79	19	NF	10	B	B
63	930509	01:28	115	90	40	152	27	257	27	U	33	B	A
64	930510	18:30	80	70	30	117	5	211	35	SS	18	A	A
65	930514	21:25	125	60	80	132	14	280	73	TF	15	A	A
66	930521	19:01	275	25	60	117	22	329	64	TF	9	A	A
67	930524	11:50	260	80	−30	123	28	221	13	SS	13	A	A
68	930602	20:04	150	65	110	135	17	3	64	TF	10	A	A
69	930626	17:47	155	60	110	140	12	15	68	TF	19	A	A
70	930701	21:41	135	75	−40	358	38	100	14	U(NS)	13	A	A
71	930701	21:23	325	85	60	350	33	116	42	U	11	A	A
72	930703	03:36	50	65	−140	179	45	83	6	NS	10	A	B
73	930709	15:51	150	75	0	15	10	284	10	SS	15	B	B
74	930728	21:28	150	60	110	135	12	10	68	TF	19	A	A
75	930730	18:40	85	50	−10	321	33	216	21	U(SS)	15	B	A
76	930810	01:14	230	60	−50	103	55	202	6	NF	20	B	A
77	930811	14:46	170	30	−60	106	66	328	17	NF	14	A	A
78	930824	01:20	210	45	−100	303	82	37	0	NF	11	A	A
79	931012	20:21	55	55	60	75	5	177	65	TF	21	A	A
80	931018	07:25	165	45	−150	305	14	52	48	TS	12	A	A
81	940223	08:33	40	90	50	72	32	187	32	U	11	A	A
82	940223	23:57	230	20	−70	197	63	34	25	NF	12	A	A
83	940228	20:43	225	45	50	72	6	329	62	TF	15	A	A
84	940326	13:25	215	85	−40	74	30	178	23	U	15	B	A
85	940421	15:07	170	75	−50	29	44	141	19	NS	11	B	A
86	940421	17:05	80	5	120	232	40	47	49	U	8	A	B

Table IV (*continued*).

No.	Date	Orig. time	Strike	Dip	Rake	*P* azim.	Axes plun.	*T* azim.	Axes plun.	F.P.S. classes	Pol. num.	Q_f	Q_p
87	940421	19:28	195	70	170	330	7	63	20	SS	16	B	A
88	940504	14:13	165	45	−150	277	48	24	14	NS	9	A	B
89	940506	19:09	155	40	−140	256	56	9	14	NF	27	A	A
90	940601	02:43	275	80	−70	117	51	258	32	U(NF)	15	A	A
91	940608	23:49	110	55	−110	239	71	124	7	NF	14	B	A
92	940611	04:09	90	70	−30	318	35	52	5	SS	10	A	A
93	940621	05:56	240	35	−90	240	80	59	10	NF	12	A	A
94	940621	09:01	290	40	−20	177	44	63	22	U(NS)	11	A	A
95	940707	14:03	45	90	170	0	7	269	7	SS	19	A	B
96	940708	05:36	105	60	−170	233	27	330	14	SS	11	A	B
97	940714	02:42	235	80	130	205	24	92	41	U	10	A	B
98	940714	03:18	225	80	170	0	0	90	14	SS	9	A	B
99	940717	11:18	185	60	60	206	10	315	62	TF	7	A	A
100	940723	20:57	195	40	150	334	18	88	50	TS	14	A	A
101	940808	17:38	100	55	−130	220	58	127	2	NF	17	A	A
102	940808	19:48	30	75	−110	184	55	45	27	NF	17	A	A
103	940819	01:51	200	50	−80	72	81	192	4	NF	13	A	A
104	940823	20:00	55	90	70	73	41	216	41	U	12	A	B
105	940908	02:39	70	55	−120	192	65	90	5	NF	18	A	A
106	940910	13:19	100	55	−60	337	65	79	5	NF	13	A	B
107	940920	19:10	175	75	−90	355	60	175	30	NF	18	B	B
108	940926	19:28	195	80	−40	56	34	160	18	SS	8	A	B
109	940926	19:38	30	80	40	64	18	168	34	SS	13	A	B
110	940926	19:43	145	85	−130	290	36	176	28	U	10	A	B
111	940926	21:08	130	75	−110	284	55	145	27	NF	8	A	A
112	940926	21:20	195	65	−10	64	24	329	10	SS	13	A	A
113	940926	21:49	185	85	−50	39	36	153	28	U	12	A	A
114	940926	22:48	170	65	50	197	11	302	52	TF	10	A	A
115	940927	00:26	210	60	0	79	20	340	20	SS	14	A	A
116	940929	04:25	0	90	70	18	41	161	41	U	10	B	A
117	941001	22:37	175	75	130	146	19	34	44	TS	15	A	A
118	941011	16:35	15	70	20	236	0	146	27	SS	28	A	A
119	941012	04:59	200	80	−40	61	34	165	18	SS	43	B	A
120	941016	21:52	265	80	170	40	0	130	14	SS	14	A	A
121	941019	11:09	15	70	0	241	13	148	13	SS	13	A	A
122	941020	13:25	85	75	−30	310	31	46	9	SS	9	A	A
123	941112	21:35	90	55	−90	270	80	90	10	NF	8	A	B
124	941127	07:26	70	40	−130	164	62	277	11	NF	27	A	A
125	941127	07:30	230	75	−170	3	17	94	3	SS	9	A	B
126	941211	18:22	140	90	20	183	13	276	13	SS	12	A	B
127	950210	08:15	175	65	10	40	10	305	24	SS	24	A	A
128	950211	02:12	225	55	−20	101	37	2	11	SS	10	A	A
129	950308	08:55	135	15	−110	162	58	331	30	NF	18	B	A
130	950405	20:29	280	70	−20	148	27	58	0	SS	14	A	A

Table IV (*continued*).

No.	Date	Orig. time	Strike	Dip	Rake	P azim.	Axes plun.	T azim.	Axes plun.	F.P.S. classes	Pol. num.	Q_f	Q_p
131	950411	12:06	260	80	30	298	13	36	28	SS	21	A	B
132	950517	15:47	130	30	10	6	33	239	42	U	6	A	A
133	950529	06:52	140	40	130	292	11	45	62	TF	28	A	A
134	950531	00:21	85	85	−30	307	24	45	16	SS	12	A	A
135	950605	22:26	70	55	−140	190	51	282	1	NS	21	B	B
136	950607	03:49	210	85	90	210	40	30	49	U	12	A	B
137	950613	07:37	150	50	−160	270	39	13	15	U(NS)	17	A	A
138	950613	16:00	170	30	−120	233	66	11	17	NF	8	A	A
139	950627	01:44	255	70	0	121	13	28	13	SS	11	A	A
140	950723	18:44	195	65	70	209	17	341	64	TF	29	B	A
141	950724	16:58	245	55	−50	124	58	217	2	NF	16	A	A
142	950725	23:01	85	50	50	292	2	198	60	TF	8	A	B
143	950726	03:18	200	45	−120	300	68	40	3	NF	11	A	B
144	950803	12:15	165	5	−40	110	48	298	41	U	8	A	A
145	950806	21:12	90	75	−150	280	73	54	11	NF	19	B	A
146	950807	01:02	130	80	−10	255	46	37	36	U	19	B	A
147	950807	01:23	115	40	−170	357	58	113	14	NF	18	B	A
148	950815	01:05	140	80	140	105	18	1	34	SS	9	A	B
149	950827	19:42	140	75	60	162	24	286	50	U(TF)	21	B	A
150	950830	21:11	90	80	0	315	7	224	7	SS	6	A	B
151	950830	23:52	65	15	60	298	17	29	3	SS	11	A	A
152	950918	21:00	230	40	−70	152	75	35	6	NF	11	A	A
153	950918	21:05	235	30	160	59	3	328	17	SS	16	A	A
154	950919	05:30	235	60	−140	0	48	267	2	NS	8	A	A
155	950920	16:24	120	50	−120	62	65	164	5	NF	14	A	A
156	950924	22:59	265	50	−60	152	67	244	0	NF	7	A	A
157	950924	23:43	170	65	130	142	11	37	52	TF	10	A	A
158	950930	10:14	210	80	−170	355	8	74	0	SS	28	A	A
159	951003	05:30	130	40	120	289	8	42	69	TF	10	A	A
160	951003	20:48	150	65	−30	0	16	262	24	SS	14	A	A
161	951004	02:00	170	70	10	166	56	279	14	NF	22	A	A
162	951005	23:51	120	55	−170	106	60	263	27	NF	26	A	A
163	951014	03:41	75	75	−150	209	31	113	9	SS	9	A	B
164	951022	07:33	135	65	−160	100	59	286	30	NF	15	A	A
165	951104	14:16	195	40	120	354	8	107	69	TF	7	A	A
166	951108	09:45	165	15	−150	122	67	214	0	NF	25	A	A
167	951108	14:20	170	70	−40	172	24	74	16	SS	18	A	A
168	951120	05:44	205	35	30	0	3	270	10	SS	7	A	B
169	951202	17:19	175	65	−70	28	64	160	17	NF	11	A	A
170	951208	16:21	105	50	160	197	81	327	5	NF	12	A	A
171	951223	15:41	285	85	−40	144	30	248	23	U	6	A	A
172	951224	01:31	195	80	100	186	34	27	53	TF	9	A	B
173	951228	22:11	65	80	−110	222	51	81	32	U(NF)	12	A	A

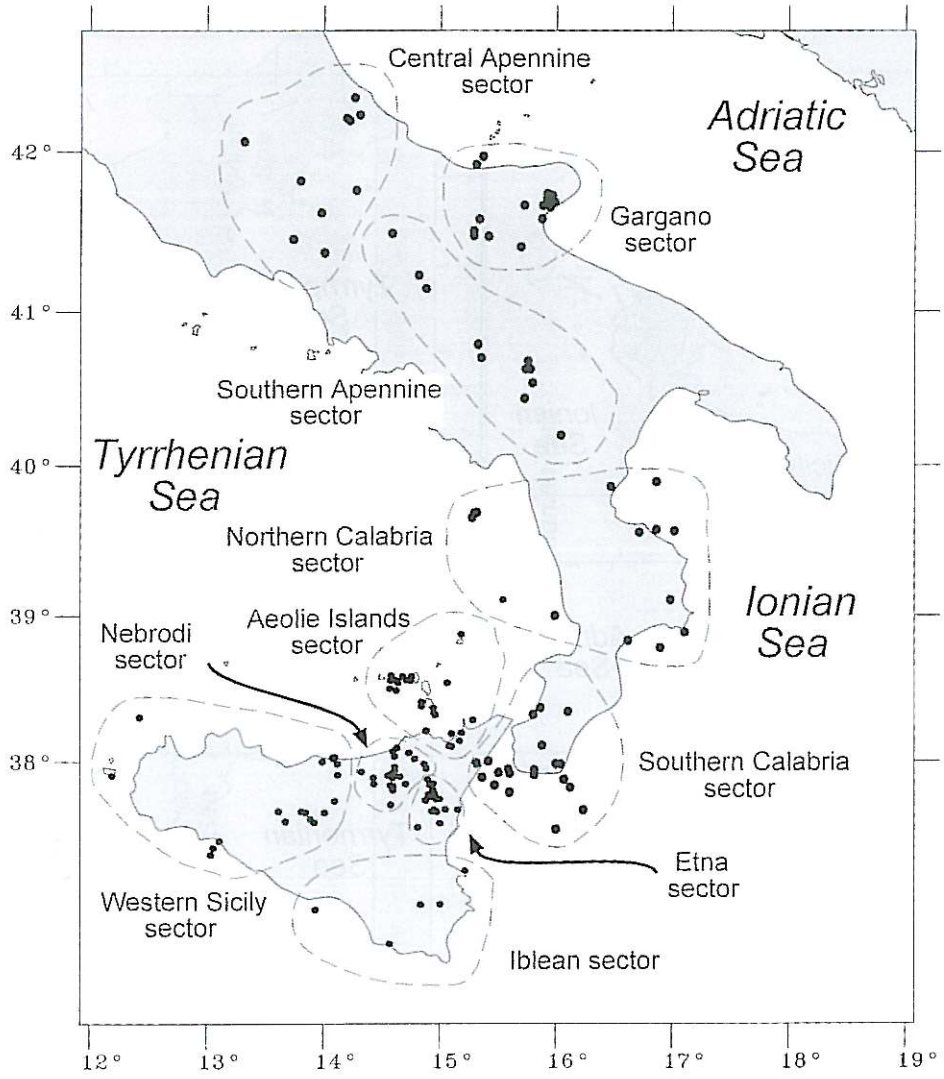

Fig. 5. Epicentral distribution of the 173 events with focal mechanisms selected in this study. The events are grouped in different geographic sectors as indicated by the dotted lines (see text for details).

occurred in the studied period (also earthquakes with rejected fault-plane solution) are grouped into three clusters. Most of these events belong to the second half of 1995. A large number of earthquakes are concentrated in the area immediately north of the Mattinata Fault. The other two clusters are one offshore between the Northern Gargano coast and the Tremiti Islands and the other to the NW of Foggia. Magnitudes range between 2.8 and 4.4. Focal depths are mostly concentrated between 14 and 24 km. Many of these solutions have *T*-axes oriented E-W and NE-SW. The two solutions to the south of the Tremiti Islands (one NF and one SS) show a NNW-SSE *T*-axes.

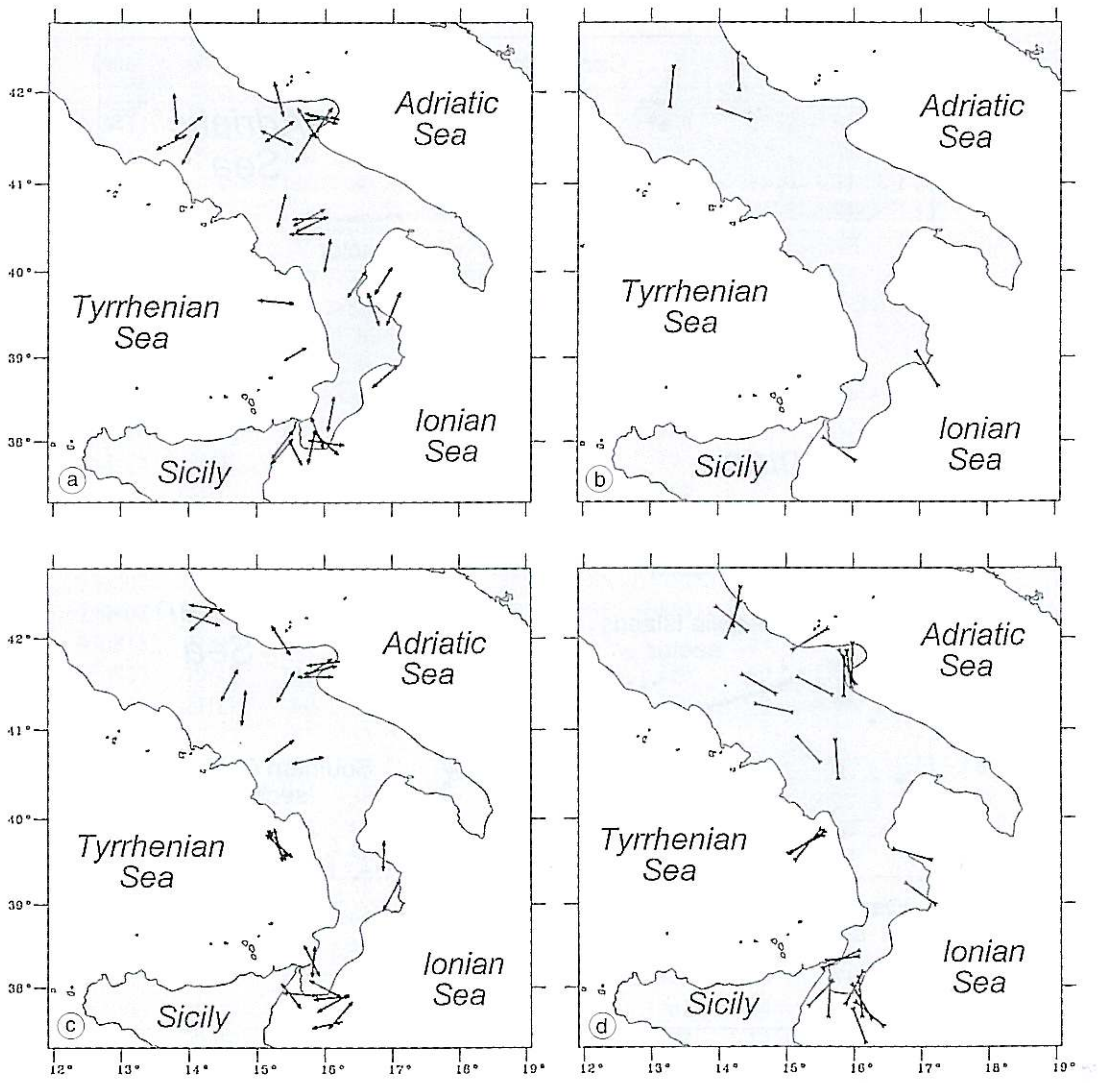

Fig. 6a-d. Distribution of *P*- and *T*-axes of the selected fault-plane solutions of the Southern Apennines and Calabrian arc. a) *T*-axes of normal solutions (NF-NS categories); b) *P*-axes of thrust solutions (TF-TS); c) *T*-axes of strike-slip solutions (SS); d) *P*-axes of strike-slip solutions (SS).

3.4. *Northern Calabria sector*

In this sector we have 17 focal mechanisms, seven of which are NF, six SS, one TF and three U solutions. Nine events are concentrated along the Ionian coast of Calabria in which the NF solutions are prevalent. In general *T*-axes of the NF and SS solutions are NNE-SSW and NE-SW oriented. The *P*-axis of the only TF solution is NW-SE as is that of the two SS solutions. Along the Calabrian eastern coast magnitudes range between 2.8 and 4.0, and hypocentral

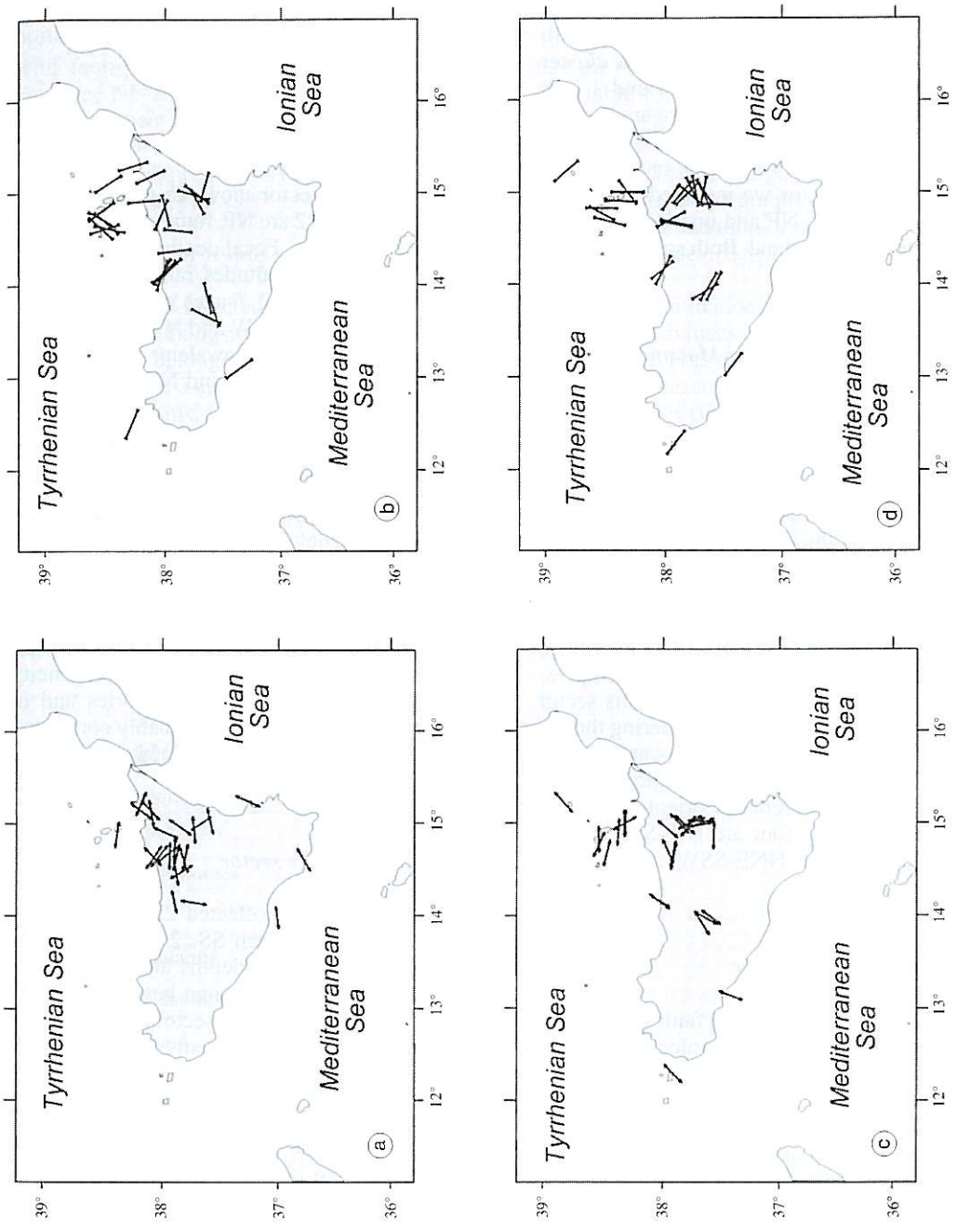

Fig. 7a-d. Distribution of P- and T-axes of the selected fault-plane solutions of the Sicilian region. a), b), c) and d) as in figure 6a-d.

depth are in the upper 15 km except event number 84 (table I) in the Squillace Gulf which is 27 km deep. The Policastro Gulf cluster in the Tyrrhenian Sea is characterized by five events with magnitudes between 3.2 and 4.1. In this cluster hypocentral depth is shallower (around 1 km) except for one event (11 km). There are four SS solutions and only one NF. For the SS solutions *T*-axes are NW-SE and for the NF one it is E-W oriented. In this sector we included two fault-plane solutions (one NF and one U) located to the NE of Stromboli Island. Both solutions show a ENE-WSW *T*-axis.

3.5. *Southern Calabria and Messina Strait sector*

The focal mechanisms selected in this sector are 21: eight NF, nine SS, one TF and three U. Focal depths are between 8 and 17 km. Only five earthquakes located in the Ionian Sea (south and south-east of the Calabrian coast) are deeper and show depths from 18 to 32 km. Probably these events are connected with the subduction process of the Ionian plate. In fact all these solutions (which are three SS and one TF) have a NW-SE *P*-axes indicating an active compression. Magnitude of all the events in this sector ranges between 2.6 and 3.8. Considering the NF and SS solutions of the events located in the Messina Strait and Aspromonte region, we observed a quite heterogeneous orientation of *T*-axes: three are E-W, four are NW-SE, two are NNW-SSE, four are NNE-SSW and two are NE-SW.

3.6. *Aeolian Islands sector*

In this sector we have 24 fault-plane solutions. The TF solutions are prevalent (10), while SS, NF and U are 8, 5 and one, respectively. Hypocentral depths are concentrated between 10 and 20 km. Only three events have a depth between 20 and 26 and two show depths less than 10 km. Magnitudes range between 2.5 and 4.4. Part of the events of this sector are located beneath the Northeastern Sicilian coast. The TF and SS solutions show *P*-axes mostly oriented N-S and NNW-SSE, while the general trend of *T*-axes of NF and SS solutions is E-W. Only two NF solutions along the Northeastern Sicilian coast show NE-SW *T*-axes as one SS solution close to Stromboli Island.

3.7. *Nebrodi sector*

The Nebrodi sector shows 25 fault-plane solutions of which 12 are NF, four SS, four TF and five are U solutions. Focal depths are between 4 and 27 km and magnitudes range from 2.6 to 3.8. The orientation of *T*-axes of NF and SS is very heterogeneous. E-W and NW-SE trends of orientation seem to be prevalent. *P*-axes of TF and SS solutions are N-S and NW-SE.

3.8. *Etna sector*

As in the Nebrodi sector also this sector shows a large heterogeneity in *P*- and *T*-axes orientation. We selected 21 focal mechanisms. Nine solutions are SS, four NF, four TF and four are U. Magnitudes range between 2.5 and 3.7 and hypocentral depth are in large part concentrated in the upper 15 km. The heterogeneity both in fault-plane solution categories and in *P*- and *T*-axes orientation is probably connected with the volcanic processes characterizing this sector.

3.9. *Western Sicily sector*

In this sector we selected 22 focal mechanisms: 11 are TF, seven SS, 2 NF and two U solutions. Hypocentral depths are in the upper 25 km and magnitudes range between 2.8 and 4.3. The seismicity in this sector is spread over a large area. The nine events of the Pollina cluster are shallower with focal depths between 2 and 6 km. The six TF and the two SS solutions of this cluster have NW-SE *P*-axes. The general trend of *P*-axes orientation relative to both TF and SS solutions in all this sector is NW-SE. Only three events in the central portion of the island (TF solutions) show a NE-SW *P*-axes.

3.10. *Iblean sector*

The seismicity during the studied period was very poor in this sector. Only five earthquakes with fault-plane solutions are selected. There are three NF and two U solutions. Magnitudes range between 3.0 and 3.8 and focal depths are in the upper 15 km. The three NF solutions show *T*-axes approximately NE-SW oriented.

3.11. *Summary of results*

Globally, we selected 173 fault plane solutions (fig. 4) among which 22 were discarded because they belong to the unknown category (oblique *P*- and *T*-axes). Of the remaining 151 focal mechanisms, we have 60 normal faulting earthquakes (40% of the total), 57 strike-slip solutions (38%), and only 34 thrust faulting events (22% of the total). This means that in general normal faulting (or a combination of normal faulting and strike-slip) dominates in Southern Italy, and that reverse faulting is less frequent (22%). Moreover, if we look at the areal distribution of thrust faulting earthquakes, we notice that they occur only in specific regions (figs. 6a-d and 7a-d), namely the Central Apennines, the Ionian coastal region of Calabria, Northern and Western Sicily. In particular, the two regions where thrust faulting dominates are the Aeolian Islands area (10 TF, 8 SS and 5 NF; table V), Central and Western Sicily (11 TF, 7 SS and 2 NF). Strike-slip faulting prevails only in the Etna region (4 NF, 9 SS and 4 TF), where we observe a high degree of heterogeneity (also 4 U events are present). In all the other regions a combination of normal and strike-slip faulting includes 70 to 100% of the focal mechanisms.

The determination of the stress field within different provinces of Italy by applying the Gephart and Forsyth (1984) method on both the data of the present study and those of the Northern Apennines (Frepoli and Amato, 1997) is the object of a specific paper (Frepoli and Amato, 2000). In that paper we focus on the significance of small earthquake fault plane solutions to retrieve the stress tensor in large regions with sparse seismicity. It appears that the stress inversion results for most of the regions analyzed are geologically sound and consistent with other data, although they are often characterized by relatively large misfit values.

Table V. Number of events grouped by fault plane solution categories for each geographic sector.

	Geographic sectors	NF	SS	TF	U
1	Central Apennines	4	3	3	–
2	Southern Apennines	6	4	–	1
3	Gargano	9	7	–	1
4	Northern Calabria	7	6	1	3
5	Southern Calabria and Messina Strait	8	9	1	3
6	Aeolian Island	5	8	10	1
7	Nebrodi	12	4	4	5
8	Etna	4	9	4	4
9	Western Sicily	2	7	11	2
10	Iblean	3	–	–	2
Total		60	57	34	22